Corrections

PHYSICS

Correction for "Quantitative field theory of the glass transition," by Silvio Franz, Hugo Jacquin, Giorgio Parisi, Pierfrancesco Urbani, and Francesco Zamponi, which appeared in issue 46, November 13, 2012, of *Proc Natl Acad Sci USA* (109: 18725–18730; first published October 29, 2012; 10.1073/pnas.1216578109).

On page 18727, right column, Eq. **12** should instead appear as

$$\Gamma[\{\phi_{ab}\}] = \frac{1}{2}\int \frac{\mathrm{d}p}{(2\pi)^D}\left(\sum_{a\neq b}(\mu\sqrt{\epsilon}+\sigma p^2)|\phi_{ab}(p)|^2 + m_2\sum_a\Big|\sum_b \phi_{ab}(p)\Big|^2 + m_3\Big|\sum_{a\neq b}\phi_{ab}(p)\Big|^2\right) + \frac{w_1}{6}\int \sum_{a\neq b\neq c\neq a}\frac{\mathrm{d}p\mathrm{d}p'}{(2\pi)^{2D}}\phi_{ab}(p)\phi_{bc}(p')\phi_{ca}(-p-p') + \frac{w_2}{6}\int\sum_{a\neq b}\frac{\mathrm{d}p\mathrm{d}p'}{(2\pi)^{2D}}\phi_{ab}(p)\phi_{ab}(p')\phi_{ab}(-p-p'), \quad [12]$$

On page 18728, right column, Eq. **21** should instead appear as

$$\lambda = \frac{1}{2}\frac{\frac{1}{\rho^4}\int \mathrm{d}x\frac{k_0^3(x)}{\tilde{g}^2(x)}}{\frac{1}{\rho^3}\int\frac{\mathrm{d}q}{(2\pi)^D}k_0^3(q)[1-\rho\Delta c(q)]^3} \quad [21]$$

The authors note that Tables 1 and 2 appeared incorrectly. The corrected tables appear below.

Table 1. Numerical values of the coefficients of the effective action and the physical quantities from the HNC approximation

System	T	ρ_d	$-w_1$	$-w_2$	m_2	m_3	σ	μ	λ	ξ_0	G_0	Gi
SS-6	1	6.691	$3.88\cdot10^{-6}$	$1.35\cdot10^{-6}$	-0.000925	0.000110	0.000195	0.000525	0.348	0.601	224	0.0267
SS-9	1	2.912	0.0000772	0.0000272	-0.00539	0.000633	0.00163	0.00543	0.353	0.548	34.3	0.0125
SS-12	1	2.057	0.000275	0.0000973	-0.0116	0.00132	0.00378	0.0152	0.354	0.498	14.2	0.0118
LJ	0.7	1.407	0.00106	0.000376	-0.0258	0.00290	0.00989	0.0414	0.355	0.489	6.00	0.00833
HarmS	10^{-3}	1.336	0.00129	0.000465	-0.0336	0.00343	0.00772	0.0779	0.359	0.315	2.82	0.0434
HarmS	10^{-4}	1.196	0.00165	0.000622	-0.0403	0.00386	0.00819	0.109	0.378	0.274	1.69	0.0632
HarmS	10^{-5}	1.170	0.00174	0.000663	-0.0416	0.00395	0.00845	0.109	0.382	0.278	1.66	0.0635
HS	0	1.169	0.00174	0.000664	-0.0418	0.00397	0.00847	0.108	0.381	0.280	1.67	0.0639

For each potential, lengths are given in units of r_0 and energies in units of ε, with $k_B = 1$. Data at fixed temperature, using density as a control parameter with $\epsilon = \rho_d - \rho$.

Table 2. Same as Table 1, but here the data are at fixed density, using temperature as a control parameter with $\epsilon = T_d - T$

System	ρ	T_d	$-w_1$	$-w_2$	m_2	m_3	σ	μ	λ	ξ_0	G_0	Gi
LJ	1.2	0.336	0.00186	0.000663	-0.0361	0.00403	0.0147	0.0572	0.356	0.507	4.56	0.00730
LJ	1.27	0.438	0.00153	0.000541	-0.0321	0.00370	0.0128	0.0447	0.353	0.536	5.74	0.00771
LJ	1.4	0.684	0.00108	0.000383	-0.0260	0.00293	0.0100	0.0292	0.355	0.586	8.52	0.00825
WCA	1.2	0.325	0.00195	0.000686	-0.0389	0.00426	0.0133	0.0607	0.351	0.467	4.37	0.0134
WCA	1.4	0.692	0.00111	0.000388	-0.0270	0.00301	0.00966	0.0291	0.350	0.576	8.67	0.0106

www.pnas.org/cgi/doi/10.1073/pnas.1309463110

CHEMISTRY, BIOPHYSICS AND COMPUTATIONAL BIOLOGY

Correction for "Probing the relative orientation of molecules bound to DNA through controlled interference using second-harmonic generation," by Benjamin Doughty, Yi Rao, Samuel W. Kazer, Sheldon J. J. Kwok, Nicholas J. Turro, and Kenneth B. Eisenthal, which appeared in issue 15, April 9, 2013, of *Proc Natl Acad Sci USA* (110:5756–5758; first published March 25, 2013; 10.1073/pnas.1302554110).

The authors note that the following statement should be added to the Acknowledgments: "We also acknowledge funding from the Chemical Sciences, Geosciences and Bioscience Division, Office of Basic Energy Sciences, Office of Science of the US Department of Energy."

www.pnas.org/cgi/doi/10.1073/pnas.1310422110

IN THIS ISSUE

Correction for "In This Issue," which appeared in issue 21, May 21, 2013, of *Proc Natl Acad Sci USA* (110:8315–8316; 10.1073/iti2113110).

The authors note that within "Measuring telomeres in single cells" on page 8316 the writing credit "C.R." should instead appear as "C.B." The online version has been corrected.

www.pnas.org/cgi/doi/10.1073/pnas.1310833110

NEUROSCIENCE

Correction for "Progressive dopaminergic cell loss with unilateral-to-bilateral progression in a genetic model of Parkinson disease," by Maxime W. C. Rousseaux, Paul C. Marcogliese, Dianbo Qu, Sarah J. Hewitt, Sarah Seang, Raymond H. Kim, Ruth S. Slack, Michael G. Schlossmacher, Diane C. Lagace, Tak W. Mak, and David S. Park, which appeared in issue 39, September 25, 2012, of *Proc Natl Acad Sci USA* (109:15918–15923; first published September 10, 2012; 10.1073/pnas.1205102109).

The authors note that the incorrect term appeared for the mice background that they used. All instances of "C57BL/6J" should instead appear as "C57BL/6." The locations were:

On page 15918, left column, line 4 within the Abstract
On page 15918, right column, first full paragraph, line 5
On page 15922, left column, second full paragraph, line 2

These errors do not affect the conclusions of the article.

www.pnas.org/cgi/doi/10.1073/pnas.1310560110

Progressive dopaminergic cell loss with unilateral-to-bilateral progression in a genetic model of Parkinson disease

Maxime W. C. Rousseaux[a], Paul C. Marcogliese[a], Dianbo Qu[a], Sarah J. Hewitt[a], Sarah Seang[a], Raymond H. Kim[b], Ruth S. Slack[a], Michael G. Schlossmacher[c,d], Diane C. Lagace[a], Tak W. Mak[b], and David S. Park[a,e,1]

[a]Department of Cellular and Molecular Medicine, University of Ottawa, Ottawa, ON, Canada, K1H 8M5; [b]Campbell Family Institute for Breast Cancer Research, Department of Medical Biophysics, University of Toronto, Toronto, ON, Canada, M5G 2C1; [c]Division of Neurology, Department of Medicine, Ottawa Hospital, Ottawa, ON, Canada, K1H 8M5; [d]Division of Neuroscience, Ottawa Hospital Research Institute, Ottawa, ON, Canada, K1H 8M5; and [e]Department of Cogno-Mechatronics Engineering, Pusan National University, Geumjeong-gu, Busan 609-735, South Korea

Edited by Thomas C. Südhof, Stanford University School of Medicine, Stanford, CA, and approved August 10, 2012 (received for review March 26, 2012)

DJ-1 mutations cause autosomal recessive early-onset Parkinson disease (PD). We report a model of PD pathology: the DJ1-C57 mouse. A subset of DJ-1–nullizygous mice, when fully backcrossed to a C57BL/6J background, display dramatic early-onset unilateral loss of dopaminergic (DA) neurons in their *substantia nigra pars compacta*, progressing to bilateral degeneration of the nigrostriatal axis with aging. In addition, these mice exhibit age-dependent bilateral degeneration at the *locus ceruleus* nucleus and display mild motor behavior deficits at aged time points. These findings effectively recapitulate the early stages of PD. Therefore, the DJ1-C57 mouse provides a tool to study the preclinical aspects of neurodegeneration. Importantly, by exome sequencing, we identify candidate modifying genes that segregate with the phenotype, providing potentially critical clues into how certain genes may influence the penetrance of DJ-1–related degeneration in mice.

animal model | PARK7 | neuritic beading | neuronal death | neuroinflammation

Parkinson disease (PD) is a progressive neurodegenerative disorder with complex symptomology and etiology affecting an ever-increasing number of individuals. Although multifactorial in nature, increasing insight has been gained with regard to the pathogenesis of PD through investigation of genes linked to the disease. Because monogenic forms of PD can be modeled in a laboratory, numerous animal models have been created to recapitulate the disease. For instance, loss-of-function mutations in the *DJ-1* (*PARK7*) gene cause early-onset autosomal recessive PD (1, 2). Patients harboring *DJ-1* mutations exhibit certain key characteristics principally in early-onset PD and may lack certain neuropathological attributes present in sporadic PD cases such as Lewy bodies (LBs) (3). However, generation of DJ-1–nullizygous mice (DJ-$1^{-/-}$) on mixed background by various laboratories, including our own, failed to detect any basal levels of neurodegeneration even in aged mice (4–11) (see Table S1). Similarly, a number of PD-related, genetically manipulated mice have been created in attempts to recapitulate the disease process, whereas little or none has shown clear or robust neurodegeneration specific to the *substantia nigra pars compacta* (SNc) (reviewed in ref. 12). Therefore, the creation of murine PD models that demonstrate significant dopaminergic (DA) loss remains an acute need in the field. The need for an early-onset model of PD is made more pressing given that no postmortem analyses of human DJ-1 mutant-carrying patients have been reported. This is particularly critical if we are to understand how specific signaling pathways govern DA loss in monogenic forms of early-onset human PD. Presently, most mechanistic studies of DA loss rely on acute toxin models of Parkinsonism. However, the relevance of such studies to the human condition remains uncertain, because acute neurotoxins are rarely the culprit in the majority of PD cases. This potential discrepancy is highlighted by a number of failed clinical trials that have heavily relied on toxin models as preclinical evidence for efficacy (13–16). A more representative model of DA loss that uses known factors in human PD is likely vital to develop better therapeutic outcomes.

Results

In the course of our studies examining the effects of environmental perturbations in DJ-$1^{-/-}$ mice, we continued to examine the long-term effects of DJ-1 deficiency on DA neuron loss. Importantly, this was accomplished in animals completely backcrossed onto a C57BL/6J background (14× backcrossed, DJ-$1^{-/-}$; herein, referred to as DJ1-C57). Intriguingly, unilateral SNc degeneration in a subset of these DJ1-C57 knockout mice is observed as early as 2 mo of age (Fig. 1*A*, Fig. S1, and Table S2). This phenotype is not observed in animals younger than 2 mo ($n = 8$; Fig. S1), thus indicating that this defect is unlikely to be developmental in origin. Moreover, this phenotype is not observed in any of the wild-type (WT) mice examined ($n = 71$). In addition, the ventral tegmental area (VTA) of these mice is mostly spared (Fig. 1*D*). This latter finding is particularly interesting given the observation that in postmortem brains from PD patients, VTA neurons remain relatively protected compared with their nigral counterparts (17).

To objectively assess this phenotype, mice in this study are classified as either "affected" (unilateral phenotype: having a greater than 40% unilateral reduction of DA cells in the SNc compared with the other side) or "unaffected" (no unilateral phenotype: having similar bilateral DA cell numbers). No clear side or sex specificity is observed (right, 53%; female, 67%, respectively). Thus, to maintain consistency, "side A" is the term given for the side of the brain with the least number of neurons, regardless of the genotype (side B being the side with more DA neurons). When quantified, affected DJ1-C57 mice exhibit a dramatic reduction of neurons in their SNc, as visualized by tyrosine hydroxylase (TH) and cresyl violet (CV) staining (Fig. 1*B* and *C* and see Fig. 3*A*). Upon closer magnification of the SNc, the affected DJ1-C57 mice exhibit TH-positive fiber

Author contributions: M.W.C.R. and D.S.P. designed research; M.W.C.R., P.C.M., D.Q., S.J.H., and S.S. performed research; R.H.K., R.S.S., M.G.S., D.C.L., and T.W.M. contributed new reagents/analytic tools; M.W.C.R. and P.C.M. analyzed data; and M.W.C.R. and D.S.P. wrote the paper.

The authors declare no conflict of interest.

This article is a PNAS Direct Submission.

Freely available online through the PNAS open access option.

Data deposition: The sequences reported in this paper have been deposited in the Mouse Genome Informatics (MGI) database, ftp://ftp.informatics.jax.org/pub/datasets/index.html.

[1]To whom correspondence should be addressed. E-mail: dpark@uottawa.ca.

This article contains supporting information online at www.pnas.org/lookup/suppl/doi:10.1073/pnas.1205102109/-/DCSupplemental.

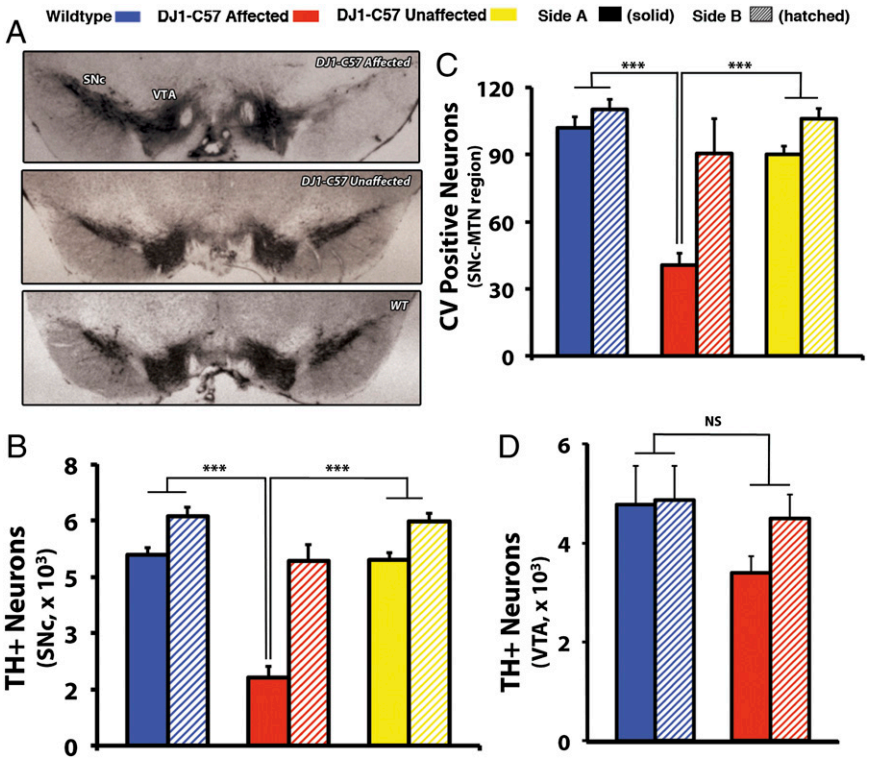

Fig. 1. Young affected DJ1-C57 mice exhibit selective unilateral degeneration in their SNc. (*A*) Representative midbrain sections of DJ1-C57 affected (*Top*), DJ1-C57 Unaffected (*Middle*), and WT (*Bottom*) mice depicting TH staining in the SNc and VTA. (*B* and *C*) Quantification of *A* by stereology of total number of TH-positive cells in the SNc (*B*) and of CV-stained cells at the level of the MTN in the SNc (*C*). (*D*) Quantification of TH-positive neurons in the VTA of WT and DJ-1 affected mice. Note that WT, DJ1-C57 affected and DJ1-C57 unaffected are represented by blue, red, and yellow bars, respectively. Side A is depicted as solid shading and side B as hatched shading. NS, not significant ($P > 0.05$); ***$P < 0.001$; ANOVA, followed by Tukey's LSD post hoc tests. Data are represented as means (n = 7–80 per group) ± SEM.

staining but with clear neuronal process disruption. When quantified, the remaining fibers at the level of the SNc in the affected DJ1-C57 mice display an elevated number of shortened processes with obvious neuritic beading (Fig. 2*A*) compared with unaffected DJ1-C57 or control mice. Consistent with this finding, an increase in CD11b-positive microglia is noted in young, affected animals (Fig. 3*B*), whereas no clear increase in astrocytosis on the affected side is observed (Fig. S2).

To assess whether this histopathological phenotype corresponds with a functional outcome, we subjected animals to behavioral testing. However, DJ1-C57 affected mice do not exhibit a clear decrease in gross motor function at 2, 6, or 12 mo of age (Fig. S3 *A*–*C*) or any differences in drug-induced rotational behavior (Fig. S3*D*). The lack of behavioral differences may be accounted for by two observations. First, examination of the striatal DA terminals revealed no clear loss in striatal fibers in young animals (Fig. 2*B*). This finding raised the possibility that sprouting of neurites within the nigrostriatal pathway may be compensatory in young mice. This is of marked interest because we note significant sprouting of dysmorphic neurites (as seen in Fig. 2*A*) in the SNc, which may be compensating for the loss of cell bodies as reported previously (18, 19). Second, an increase in the striatal postsynaptic marker ΔFBJ murine osteosarcoma viral oncogene homolog B (ΔFosB) is observed in affected DJ1-C57 mice (Fig. 2*C*). PD patients have been shown to have up-regulated ΔFosB in their caudate/putamen (20). Moreover, ΔFosB has been shown previously to be up-regulated in toxin models of neurodegeneration such as 1-methyl-4-phenyl-1,2,3,6-tetrahydropyrindine (MPTP) and 6-hydroxydopamine (6-OHDA) as a compensatory response to a loss of DA innervation (21, 22).

With aging of DJ-1–deficient animals, an increase in the prevalence of the DJ1-C57 affected unilateral phenotype was observed over time, peaking at 12 mo of age (42.9% penetrance, Fig. 4*A* and Table S2). When only affected unilateral DJ1-C57 animals are considered, there was a clear loss in total number of SNc DA neurons even at early time points (Fig. S4). However, if all (affected and unaffected) DJ-1–deficient animals were evaluated together, the total number of DA neurons was not significantly reduced until later aging stages (15 mo). At this time, the unilateral phenotype dissipated and a more bilateral phenotype of nerve cell loss was observed (Fig. 4 *A* and *B* and Table S2). Interestingly, these aged mice, unlike at the earlier times, exhibited a decrease in DA-synthesizing TH-positive striatal terminals (Fig. 4*C*). Upon evaluation of any neuritic beading in these aged animals, we noted that although process length itself did not further change between young and aged DJ1-C57 mice (Fig. S5 *A* and *B*), aged DJ1-C57 mice exhibited a decreased number of sprouting processes in the SNc region (Fig. S5*C*). Moreover, long-term behavior testing revealed a mild motor defect in the aged (14–16 mo) DJ1-C57 mice when examined by both the grid test (Fig. 4*E*) and the pole test (males; Fig. 4*F*).

The neuropathology of PD encompasses degeneration not only of the SNc but also of other nuclei in the brainstem including the *locus ceruleus* (LC) (23). Therefore, LC of DJ1-C57 mice were examined for TH-immunoreactive cell bodies. A significant reduction in TH-positive cells of the LC was observed in aged DJ1-C57 mice compared with WT controls (Fig. 4*D*). Furthermore, because α-synuclein aberrant processing is a hallmark of idiopathic PD, we examined whether our DJ1-C57 mice exhibited altered expression or localization of the protein. No visible changes were noted in the expression of endogenous α-synuclein between DJ1-C57 mice and littermate controls (Fig. S6 *A* and *B*). In addition, upon examination of leucine-rich repeat kinase 2 (LRRK2) expression (another autosomal dominant PD-linked protein), we did not note any significant changes in expression or localization of the protein (Fig. S6*B*).

Finally, to elucidate potential mechanism(s) through which this selective neurodegeneration occurs in a subset of these DJ1-C57 mice, we performed whole-exome sequencing on affected (n = 3) and unaffected (n = 3) DJ-1-C57 mice as an approach to identify candidate modifiers (Fig. 5*A*). After filtering for coding regions and for variants found in all three affected but none of the three unaffected mice, only five candidates in coding regions were

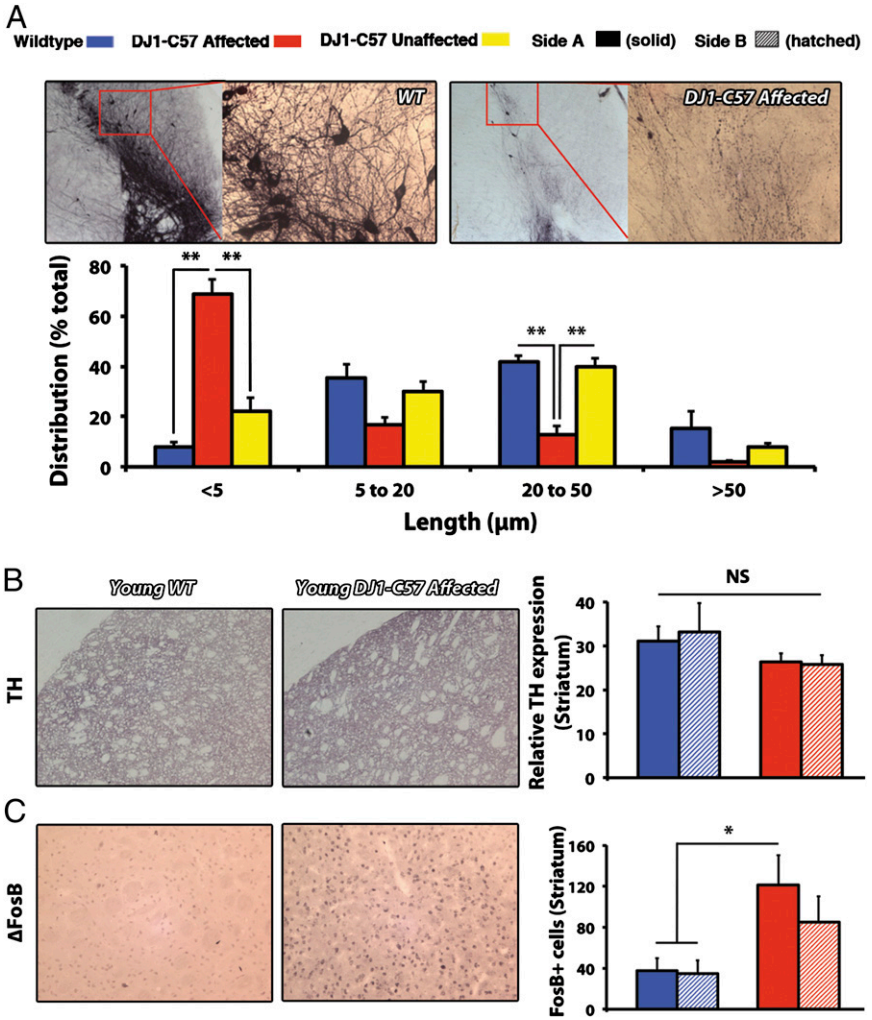

Fig. 2. Widespread process disruption and aberrant striatal innervation in young affected DJ1-C57 mice. (*A*) Fiber sprouting in WT (*Upper Left*) and DJ1-C57 affected animals (*Upper Right*). Distribution of quantified uninterrupted process (TH^+) length in a single vision plain (in microns) is presented (*Lower*). (*B*) Representative sections of striatum stained for ΔFosB in young WT (*Left*) and DJ1-C57 affected (*Center*) mice. (*Right*) Quantification of ΔFosB-positive puncta in the striatum. (*C*) Representative sections of the striatum stained for TH as in *B*. Quantification of striatal TH density is shown (*Right*). WT, DJ1-C57 affected, and DJ1-C57 unaffected are represented by blue, red, and yellow bars, respectively. Side A is depicted as solid shading and side B as hatched shading. NS, not significant ($P > 0.05$); $^*P < 0.05$; $^{**}P < 0.01$; ANOVA, followed by Tukey's LSD post hoc tests. Data are represented as means (n = 3–11 per group) ± SEM.

identified as potential modifiers of the phenotype [signal regulatory protein β (Sirbp)1A, 2610203C20Rik, zinc finger, SWIM domain containing 6 (Zswim6), kinesin family member (Kif) C5b, and SWI5-dependent recombination repair 1 (Sfr1); Fig. 5*B*]. Moreover, because exome sequencing also covers flanking intronic sequences, an additional 23 candidates were identified in noncoding regions (Table S3), although none of these were in known intron–exon splice sites. Together, these results suggest the segregation of several genomic loci with the phenotype.

Discussion

In our DJ1-C57 mice, we have uncovered an early PD-type phenotype that progressed with age and showed incomplete penetrance. In backcrossing and extensively interbreeding DJ-1–null mice, we obtained a subset of DJ1-C57 mice that exhibited robust unilateral nigral degeneration as early as 8 wk of age: a finding potentially consistent with the early-onset pathogenicity of DJ-1 loss in human carriers of DJ-1 mutations (1). This cell loss was accompanied with compensatory sprouting and the appearance of dysmorphic and beading neurites, as well as microgliosis, a result congruent with the notion that microglia may induce neuritic beading during neuronal dysfunction (24). Furthermore, findings of compensatory sprouting upon cell loss, dysmorphic neurites, and an increase in proinflammatory responses are all present in postmortem samples from PD patients (25–30). Therefore, given the early age of onset of degeneration in these mice, our findings are of particular significance and may correlate with features of autosomal recessive PD. This loss-of-function phenotype has not yet been modeled successfully in rodents, with the possible exception of a partial reduction in LC neurons in one *parkin*$^{-/-}$ mouse model (31).

We also noted that although DJ-1 loss–mediated neurodegeneration will invariably lead to PD in humans, this might not be as dramatic in mice with a relatively short lifespan of ~24 mo. However, early pathological changes associated with this genetic form of PD are nonetheless observed. Thus, much like preclinical PD, where no clear clinicopathological correlate may be apparent until over 80% of the nigral cell population has been lost, a compensatory mechanism such as neuritic sprouting or postsynaptic sensitization may account for the lack of motor defects in these young animals. Furthermore, the relevance of this model is made even more apparent as the DJ1-C57 mice

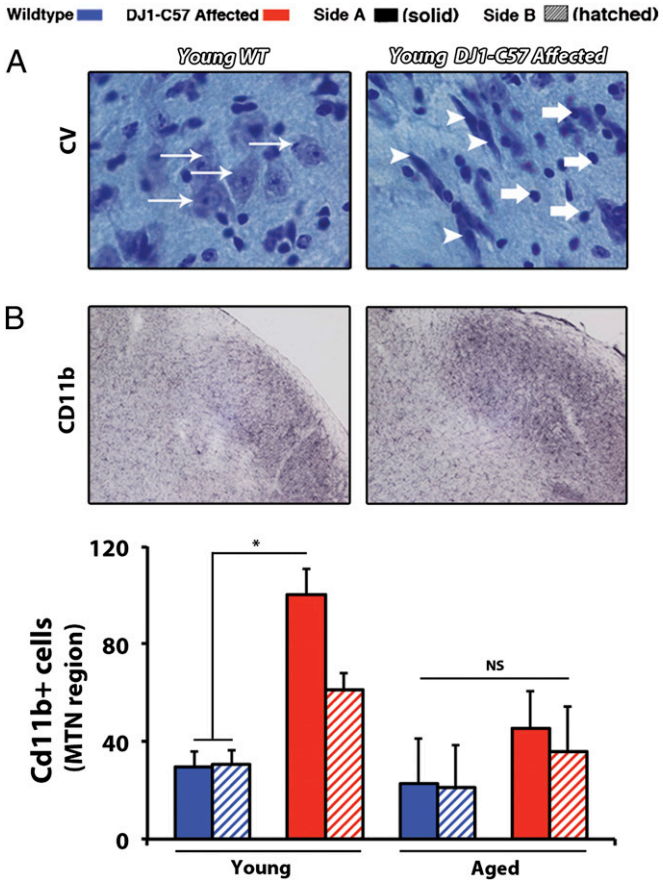

Fig. 3. Focal microgliosis in young affected DJ1-C57 mice. (*A*) Representative midbrain sections stained for CV in young WT and DJ1-C57 affected mice (1000× magnification). Thin arrows denote typical morphology of DA neurons of the SNc; thick arrows denote shrunken, dead nuclei; and arrowheads denote appearance of cells with altered morphology. (*B*) CD11b staining in the midbrain of young WT (*Left*) and DJ1-C57 affected (*Right*) mice was quantified and represented as the number of Cd11b-positive cells in the MTN region of the SNc. WT and DJ1-C57 affected are represented by blue and red bars, respectively. Side A is depicted as solid shading and side B as hatched shading. NS, not significant ($P > 0.05$); *$P < 0.05$; ANOVA, followed by Tukey's LSD post hoc tests. Data are represented as means (n = 3–9 per group) ± SEM.

age. Aged DJ1-C57 mice progressed to bilateral degeneration of their SNc, as well as of their nigrostriatal projections to the forebrain. Thus, this preclinical phenotype likely first occurs at 2 mo and progresses over the course of the following 10–12 mo. In addition, at this older stage, these mice exhibited cell loss at the level of the LC, a pathological characteristic of the human condition. Finally, aged mice beyond 12 mo start to show basal behavioral deficits. Therefore, our DJ1-C57 mouse model presents a potentially important role in filling the gap in our understanding of early-onset preclinical PD in humans.

The reason behind the observed phenotype remains unknown. To begin to explore this issue, we performed whole-exome sequencing to identify potential genes that may contain polymorphisms in affected but not unaffected mice. Surprisingly, the list of genes that met these criteria was limited to five candidates with exon-containing changes. One potential modifier gene candidate, *Sirbp1a*, was particularly interesting given the increase in microglial activation observed in the affected DJ1-C57 mice. SIRBP1A has been associated with a role in promoting phagocytosis in macrophages and monocytes (32). It is possible that disruption of this function may result in aberrant microglial activity. Future studies will seek to elucidate the putative relationship between DJ-1 and SIRBP1A, as well as with other coding modifiers. These exon candidates, although intriguing, are not the only factors that may account for the degenerative phenotype. Other possibilities include intron changes, particularly at loci-flanking

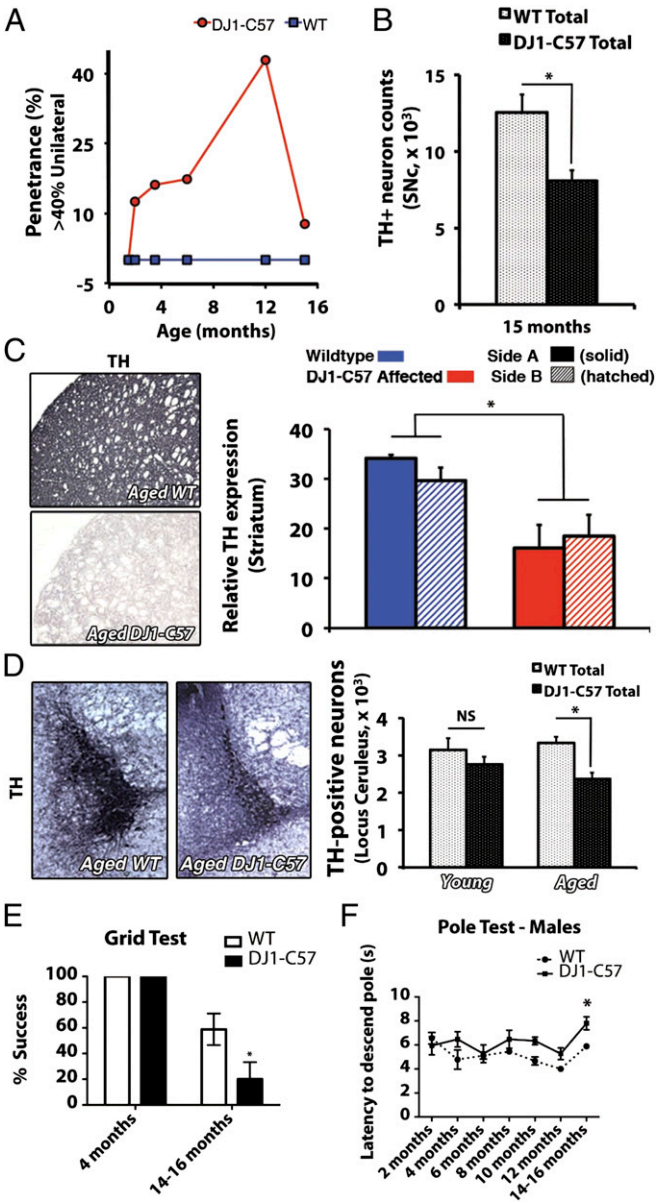

Fig. 4. Aged DJ1-C57 mice exhibit bilateral DA and noradrenergic denervation in the brainstem. (*A*) Penetrance of unilateral phenotype over time. Penetrant threshold: greater than 40% loss of DA neurons on one side (side A) vs. the other (side B). (*B*) Total stereological counts of DA neurons in the SNc of WT and DJ1-C57 aged (15-mo) animals. (*C*) Representative striatal sections of aged (12–15 mo) WT (*Upper Left*) and DJ1-C57 (*Lower Left*) mice stained for TH. Quantification of TH expression in the striatum relative to the *corpus callosum* was performed in young and aged animals (*Right*). (*D*) Representative micrographs of LC sections in the pons stained for TH for either aged WT (*Left*) or aged DJ1-C57 (*Center*). Quantification of TH-positive neurons for both young and aged animals is shown (*Right*). (*E*) The grip test evaluated the capacity of the mouse to stay on an inverted metal grid for 60 s. (*F*) The pole test evaluated the latency of mice to descend a gauze-wrapped pole (in seconds). NS, not significant ($P > 0.05$); *$P < 0.05$; ANOVA, followed by Tukey's LSD post hoc tests. Data are represented as means (n = 3–13 per group) ± SEM.

A

Genomic DNA isolation from affected/unaffected DJ1-C57 → Targeted Exome Capture (Agilent SureSelect^{XT}) → Illumina HiSeq2000 Paired end sequencing (2x100bp) → Alignment (C57Bl/6J genome) → Variant Calling (Genome Analysis Toolkit) → Identify Putative Mutations: Segregation by group

B

Gene name	Gene description	Position	Chromosome	Mutation type	Codon	Effect	Amino Acid	Function	Presence	
									Affected (/3)	Unaffected (/3)
Sirpb1a	signal-regulatory protein beta 1A	15,417,016	3	SNP	tCc/tTc	Missense Mutation	S84F	Phagocytosis	3	0
Sirpb1a	signal-regulatory protein beta 1A	15,417,020	3	SNP	Cat/Tat	Missense Mutation	H83Y	Phagocytosis	3	0
2610203C20Rik	RIKEN cDNA 2610203C20 gene	41,389,287	9	SNP	Acc/Ccc	Missense Mutation	T59P	Unknown	3	0
2610203C20Rik	RIKEN cDNA 2610203C20 gene	41,389,294	9	SNP	cAc/cCc	Missense Mutation	H61P	Unknown	3	0
Zswim6	zinc finger, SWIM domain containing 6	108,679,774	13	SNP	gCg/gGg	Missense Mutation	A157G	Unknown	3	0
Kifc5b	kinesin family member C5B	27,061,155	17	SNP	Gtc/Atc	Missense Mutation	V319I	Chromosomal segregation	3	0
Sfr1	SWI5 dependent recombination repair 1	47,807,383	19	SNP	Ccc/Acc	Missense Mutation	P93T	DNA recombination	3	0

Fig. 5. List of exonic variants unique to affected DJ1-C57 mice. (*A*) Schematic workflow of exome sequencing to determine candidate mutations in affected DJ1-C57 mice (vs. unaffected littermate controls). (*B*) Table of variants present in all three examined affected animals and no unaffected littermates. See *Experimental Procedures* for selection criteria.

exons. In this regard, we observed that 23 intronic modifiers segregated with the phenotype. The specific role of these polymorphisms/indels remains unclear, because they do not correspond to splice donor/acceptor sites. Finally, it is possible that a combination of all of these factors may contribute to the phenotype. Therefore, more careful analyses must be performed to examine among these possibilities. What is important, however, is that our studies demonstrate that a defined group of polymorphisms can segregate with our phenotype. How these factors regulate DA loss in DJ-1–deficient mice will require further analyses.

Collectively, we present a murine model that reproduces a clinically detectable phenotype owing to the modification of a PD-related gene. Affected DJ1-C57 mice display: (*i*) unilateral DA cell loss with a predilection for the SNc versus VTA as early as 2 mo of age; (*ii*) development of aberrant neuritic processes with ensuing microgliosis in the SNc and increased ΔFosB staining in the striatum at a young age; and (*iii*) progression to bilateral degeneration of the nigrostriatal axis and of the LC at an older age (model; Fig. 6), which are associated with mild motoric changes. This progression to a bilateral phenotype is of particular interest to us given the typical unilateral-to-bilateral progression of the disease in humans (33). Interestingly, no significant changes were noted in α-synuclein or LRRK2 expression, suggesting a disease process independent of Lewy body generation. These results strongly suggest that this murine model of early parkinsonism mimics autosomal recessive early-onset PD pathology, rather than that of sporadic PD (3). It, thus, provides a tool to elucidate the cascade of pathogenic changes that occurs in autosomal recessive, early-onset PD, as well as a platform to explore neuroprotective interventions in the future.

Experimental Procedures

DJ1-C57 Mouse Creation. DJ-1$^{-/-}$ mice were generated as described previously (9). Mice were subsequently backcrossed 14 times onto a pure C57BL/6J background (Charles River) to obtain DJ1-C57 mice. Animals were then interbred extensively for colony maintenance and experimentation. Animals were kept at 25 °C on a light (12 h)/dark (12 h) cycle with ad libitum access to standard rodent laboratory chow and water. Animal care was carried out in accordance with the guidelines of the Canadian Council and Care of Animals in Research and the Canadian Institutes of Health Research and was approved by the University of Ottawa Animal Care Veterinary Services.

Histology. After being perfused transcardially, mouse brains were fixed in 4% paraformaldehyde and cryoprotected as described elsewhere (34). Midbrain sections containing the SNc (40 μm), pontine sections containing LC (40 μμ), and striatal (14 μm) sections were immunostained via avidin–biotin complex staining as described previously (26).

DA Cell Survival Quantification. DA neuron survival in the SNc was blindly assessed by stereology using Stereo Investigator as described previously (26). Striatal TH quantification was performed at 200×. For each picture, five samples of striatum and one sample of corpus callosum were used for densitometric analysis. Relative intensity of immunodetection was calculated using ImageJ v.1.41o (National Institutes of Health). For each sample, three slices of striatum were used to calculate the mean striatal density.

Neuritic Beading Measurement. Neuritic beading was measured using ImageJ. Briefly, average length of uninterrupted process in a visually focused plane

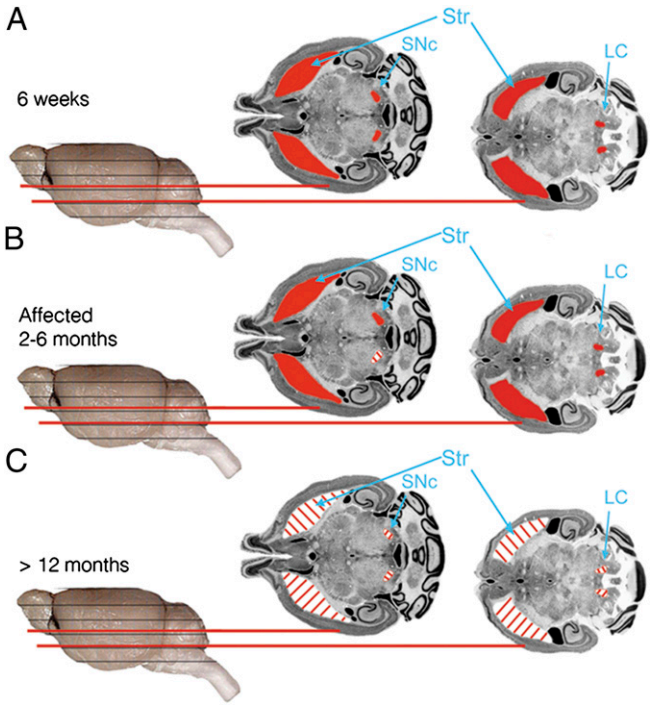

Fig. 6. DJ1-C57 preclinical model of DA neurodegeneration. (*A*) Altered representative micrographs reproduced with permission from the Mouse Brain Library [www.mbl.org; Rosen et al. (36)] depicting healthy (red) SNc, striatum, and LC in 6-wk-old DJ1-C57 mice or all WT groups examined. (*B*) Affected DJ1-C57 mice demonstrate unilateral DA cell loss in the SNc but not in the LC. (*C*) Aged DJ1-C57 mice exhibit widespread degeneration in their nigrostriatal tract, as well as their LC.

was measured as 20 measurements/section and measuring three sections per animal. Raw data were then binned into five categories of length and represented as percentage distribution.

ΔFosB and CD11b Measurement. Striatal (ΔFosB) and midbrain [cluster of differentiation (CD)11b] sections were stained, and three pictures were taken per animal, per side. Puncta in a given visual field were assessed blindly using ImageJ v1.41o.

Locus Ceruleus Neuron Quantification. Noradrenergic cell survival in the LC was measured by counting four representative sections and projecting their counts to a total value as described previously (35).

CV Quantification. CV staining and quantification were performed as described previously (26). Briefly, cell viability in the medial terminal nucleus (MTN) region of the midbrain was assessed as per the nuclear integrity of the cells present.

Antibodies Used. CD11b (1:200; AbD Serotec), FosB (1:250; Santa Cruz Biotechnologies), glial fibrillary acidic protein (GFAP) (1:1,000; Cell Signaling), DJ-1 (1:50,000; Abcam), α-synuclein (1:1,000; BD Transduction), LRRK2 (1:50,000; Epitomics), and TH (1:10,000; Immunostar or 1:2,000; Chemicon) were used for either avidin–biotin complex (ABC) visualization by 3,3′-diaminobenzidine (DAB) or via fluorophore-conjugated secondary antibody.

Motor Behavior Testing. The grid test was carried out by placing DJ1-C57 affected, unaffected, and WT mice on a metal grid (0.5-cm spacing between metal wires) and then turning the grid over for 60 s. If a mouse could hold on for the entire 60 s, it was scored as "success," whereas if it fell before the set time, it was scored as a "fail." The pole test was used to measure the latency to descent an 18-inch pole wrapped in gauze.

Exome Sequencing. Genomic DNA (6 μg) was isolated from ear samples of affected/unaffected mice using the DNeasy Blood and Tissue kit (Qiagen). Samples underwent targeted exome capture using the Agilent SureSelectXT Mouse All Exon kit and subsequently underwent next-generation sequencing via an Illumina HiSeq 2000 sequencer. Raw data were aligned to the mouse genome, and variants were called using the Broad Institute GATK (Genome Analysis ToolKit).

Statistical Analysis. Data throughout the paper are expressed as averages ± SEM for a given sample size (*n*). Statistical analysis for histological and behavioral data were performed by means of either a paired *t* test or one-way ANOVA, followed by Tukey's least significant difference (LSD) post hoc test, as indicated in *SI Text* and the figure legends.

ACKNOWLEDGMENTS. We thank the University of Ottawa Faculty of Medicine Behavior Core Facility for use of their equipment; Daniele Merico (Centre for Applied Genomics, Hospital for Sick Children) for assistance with bioinformatics analysis of the exome data; and Linda Jui, Mirela Hasu, Steve M. Callaghan, Carmen Estey, Elizabeth Abdel-Messih, and Hossein Aleyasin for technical assistance and scientific input. This work was supported by grants from Parkinson Society Canada; the Canadian Institutes of Health Research; the Centres of Excellence in Neurodegeneration (COEN); the Heart and Stroke Foundation of Ontario (HSFO); the Neuroscience Canada/Krembil Foundation; the Parkinson's Disease Foundation; The Michael J. Fox Foundation for Parkinson's Research; the Parkinson Research Consortium (PRC); the Canadian Stroke Network; the Heart and Stroke Foundation of Canada (HSFC) for Stroke Recovery; and the World Class University Program through the National Research Foundation of Korea, funded by Ministry of Education, Science, and Technology, South Korea Grant R31-2008-000-20004-0 (to D.S.P.). D.S.P. is a recipient of the HSFO Career Investigator Award. M.W.C.R. is a recipient of the HSFC Focus on Stroke Award, as well as the Canadian Institutes of Health Research (CIHR) Training Program in Neurodegenerative Lipidomics Supplement Scholarship. P.C.M. is a recipient of The PRC Toth Family Fellowship in Parkinson's Research.

1. Bonifati V, et al. (2003) Mutations in the DJ-1 gene associated with autosomal recessive early-onset parkinsonism. *Science* 299:256–259.
2. Hague S, et al. (2003) Early-onset Parkinson's disease caused by a compound heterozygous DJ-1 mutation. *Ann Neurol* 54:271–274.
3. Kitada T, Tomlinson JJ, Ao HS, Grimes DA, Schlossmacher MG (2012) Considerations regarding the etiology and future treatment of autosomal recessive versus idiopathic Parkinson disease. *Curr Treat Options Neurol* 14:230–240.
4. Ramsey CP, Tsika E, Ischiropoulos H, Giasson BI (2010) DJ-1 deficient mice demonstrate similar vulnerability to pathogenic Ala53Thr human alpha-syn toxicity. *Hum Mol Genet* 19:1425–1437.
5. Andres-Mateos E, et al. (2007) DJ-1 gene deletion reveals that DJ-1 is an atypical peroxiredoxin-like peroxidase. *Proc Natl Acad Sci USA* 104:14807–14812.
6. Chandran JS, et al. (2008) Progressive behavioral deficits in DJ-1-deficient mice are associated with normal nigrostriatal function. *Neurobiol Dis* 29:505–514.
7. Chen L, et al. (2005) Age-dependent motor deficits and dopaminergic dysfunction in DJ-1 null mice. *J Biol Chem* 280:21418–21426.
8. Goldberg MS, et al. (2005) Nigrostriatal dopaminergic deficits and hypokinesia caused by inactivation of the familial Parkinsonism-linked gene DJ-1. *Neuron* 45:489–496.
9. Kim RH, et al. (2005) Hypersensitivity of DJ-1-deficient mice to 1-methyl-4-phenyl-1,2,3,6-tetrahydropyrindine (MPTP) and oxidative stress. *Proc Natl Acad Sci USA* 102: 5215–5220.
10. Manning-Boğ AB, et al. (2007) Increased vulnerability of nigrostriatal terminals in DJ-1-deficient mice is mediated by the dopamine transporter. *Neurobiol Dis* 27:141–150.
11. Pham TT, et al. (2010) DJ-1-deficient mice show less TH-positive neurons in the ventral tegmental area and exhibit non-motoric behavioural impairments. *Genes Brain Behav* 9:305–317.
12. Dawson TM, Ko HS, Dawson VL (2010) Genetic animal models of Parkinson's disease. *Neuron* 66:646–661.
13. Parkinson Study Group PRECEPT Investigators (2007) Mixed lineage kinase inhibitor CEP-1347 fails to delay disability in early Parkinson disease. *Neurology* 69:1480–1490.
14. Waldmeier P, Bozyczko-Coyne D, Williams M, Vaught JL (2006) Recent clinical failures in Parkinson's disease with apoptosis inhibitors underline the need for a paradigm shift in drug discovery for neurodegenerative diseases. *Biochem Pharmacol* 72: 1197–1206.
15. Snow BJ, et al.; Protect Study Group (2010) A double-blind, placebo-controlled study to assess the mitochondria-targeted antioxidant MitoQ as a disease-modifying therapy in Parkinson's disease. *Mov Disord* 25:1670–1674.
16. Marks WJ, Jr., et al. (2010) Gene delivery of AAV2-neurturin for Parkinson's disease: A double-blind, randomised, controlled trial. *Lancet Neurol* 9:1164–1172.
17. Perl DP (2011) *Neuropathologic Involvement of the Dopaminergic Neuronal Systems in Parkinson's Disease* (Blackwell, Oxford), Chap 2, pp 8–10.
18. Song DD, Haber SN (2000) Striatal responses to partial dopaminergic lesion: Evidence for compensatory sprouting. *J Neurosci* 20:5102–5114.
19. Pritzel M, Huston JP, Sarter M (1983) Behavioral and neuronal reorganization after unilateral substantia nigra lesions: Evidence for increased interhemispheric nigrostriatal projections. *Neuroscience* 9:879–888.
20. Tekumalla PK, et al. (2001) Elevated levels of DeltaFosB and RGS9 in striatum in Parkinson's disease. *Biol Psychiatry* 50:813–816.
21. Doucet JP, et al. (1996) Chronic alterations in dopaminergic neurotransmission produce a persistent elevation of deltaFosB-like protein(s) in both the rodent and primate striatum. *Eur J Neurosci* 8:365–381.
22. Pérez-Otaño I, Mandelzys A, Morgan JI (1998) MPTP-Parkinsonism is accompanied by persistent expression of a delta-FosB-like protein in dopaminergic pathways. *Brain Res Mol Brain Res* 53:41–52.
23. Forno LS, Alvord EC, Jr. (1974) Depigmentation in the nerve cells of the substantia nigra and locus ceruleus in Parkinsonism. *Adv Neurol* 5:195–202.
24. Takeuchi H, et al. (2005) Neuritic beading induced by activated microglia is an early feature of neuronal dysfunction toward neuronal death by inhibition of mitochondrial respiration and axonal transport. *J Biol Chem* 280:10444–10454.
25. Greenwood CE, Tatton WG, Seniuk NA, Biddle FG (1991) Increased dopamine synthesis in aging substantia nigra neurons. *Neurobiol Aging* 12:557–565.
26. Mount MP, et al. (2007) Involvement of interferon-gamma in microglial-mediated loss of dopaminergic neurons. *J Neurosci* 27:3328–3337.
27. Ouchi Y, et al. (2005) Microglial activation and dopamine terminal loss in early Parkinson's disease. *Ann Neurol* 57:168–175.
28. McGeer PL, Itagaki S, Boyes BE, McGeer EG (1988) Reactive microglia are positive for HLA-DR in the substantia nigra of Parkinson's and Alzheimer's disease brains. *Neurology* 38:1285–1291.
29. Whitton PS (2007) Inflammation as a causative factor in the aetiology of Parkinson's disease. *Br J Pharmacol* 150:963–976.
30. Nagatsu T, Sawada M (2005) Inflammatory process in Parkinson's disease: Role for cytokines. *Curr Pharm Des* 11:999–1016.
31. Von Coelln R, et al. (2004) Loss of locus coeruleus neurons and reduced startle in parkin null mice. *Proc Natl Acad Sci USA* 101:10744–10749.
32. Hayashi A, et al. (2004) Positive regulation of phagocytosis by SIRPbeta and its signaling mechanism in macrophages. *J Biol Chem* 279:29450–29460.
33. Pahwa RLK, Koller WC (2003) *Handbook of Parkinson's Disease* (CRC, Boca Raton, FL), 3rd Ed, 597 pp.
34. Crocker SJ, et al. (2001) c-Jun mediates axotomy-induced dopamine neuron death in vivo. *Proc Natl Acad Sci USA* 98:13385–13390.
35. German DC, Liang CL, Manaye KF, Lane K, Sonsalla PK (2000) Pharmacological inactivation of the vesicular monoamine transporter can enhance 1-methyl-4-phenyl-1,2,3,6-tetrahydropyridine-induced neurodegeneration of midbrain dopaminergic neurons, but not locus coeruleus noradrenergic neurons. *Neuroscience* 101:1063–1069.
36. Rosen GD, et al. (2003) Informatics center for mouse genomics: The dissection of complex traits of the nervous system. *Neuroinformatics* 1:327–342.